COMPTES RENDUS

CHIMIE

Preliminary communication / Communication

General correlation between the chemical shift of hyperpolarized ^{129}Xenon and pore size of mesoporous solids

Elias Haddad, Andréi Nossov, Flavien Guenneau, Antoine Gédéon *

Laboratoire SIEN, UMR 7142, UPMC, tour 54, 3e étage, case 196, 75252 Paris cedex 05, France

Abstract

We report the variation of ^{129}Xe chemical shift δ versus the pore size, the temperature and the xenon pressure of xenon adsorbed on mesoporous materials prepared in different synthesis conditions. The use of hyperpolarized xenon allows us to measure spectra at very low concentration of xenon, where δ reflects mainly interaction between the adsorbed xenon atoms and the surface. We deduce the heat adsorption of xenon adsorbed on the surface of studied materials. ***To cite this article: E. Haddad et al., C. R. Chimie 7 (2004).***

Résumé

Nous présentons une étude détaillée de la variation du déplacement chimique δ du ^{129}Xe adsorbé en fonction de la taille de pores, de la température et de la pression de xénon, pour différents types de solides mésoporeux préparés dans différentes conditions de synthèse. L'utilisation du xénon hyperpolarisé nous permet de travailler avec des faibles concentrations de xénon, pour lesquelles δ dépend uniquement de l'interaction du xénon avec la surface. Nous en déduisons sa chaleur d'adsorption sur les surfaces des différents matériaux étudiés. ***Pour citer cet article : E. Haddad et al., C. R. Chimie 7 (2004).***

1. Introduction

Owing the large polarizability and the chemical inert nature of xenon, the ^{129}Xe NMR chemical shift is very sensitive to its local environment and thus provides an ideal probe and a useful tool for the investigation of the surface structure and of the adsorption sites of porous sorbents [1–5].

The sensitivity of conventional nuclear magnetic resonance NMR techniques is fundamentally limited by the ordinarily low-spin polarization achievable even in the strongest magnetic NMR magnets. However, by transferring angular momentum from circularly polarized laser light to the electronic spins of rubidium and

---

* Corresponding author.

E-mail address: ag@ccr.jussieu.fr (A. Gédéon).

Table 1
Porosity measurements, adsorption energy values (ΔH_{ads}) and xenon chemical shift on the surface (δ_s) of studied samples

Sample	S_{BET} (m^2 g^{-1})[a]	V_p (cm^3 g^{-1})[b]	D_{BJH} (Å)[c]	D_{BdB} (Å)[d]	ΔH_{ads} (kcal mol^{-1})	δ_s (ppm)
MCM-41	1062	0.8	30	34	2.08	118
AlMCM-41	971	0.81	28	31	2.13	124
SBA15-a	680	0.89	67	63	2.3	119
SBA15-b	812	0.72	38	51	2.3	125
SBA15-c	1041	1.41	55	74	1.5	125
SBA15-d	546	1.25	76	104	2.4	125
SBA15-e	909	0.76	33	44	2.2	117
SBA15-f	1030	0.66	26.6	34.5	3.15	96
SBA-16	325	0.29	35.4	46		
AlSBA-I	490	0.66	57.8	74	2.44	112
AlSBA-II	700	1.04	77.4	102	1.8	110

[a], Surface area; [b], pore volume; c, BJH pore diameter; d, BdB pore diameter [18]

then to the nuclear spins of xenon [6], optical pumping methods can increase the nuclear spin polarization of xenon by several orders of magnitude, thereby greatly enhancing its NMR sensitivity ($\times 10^4$) [7–9].

Mesoporous silicate materials consisting of an ordered network of nanometer size channels were first introduced by Mobil researchers in the early 1990s [10–11]. After a decade of intensive studies, these materials still generate strong interest in catalysis applications and adsorption [12–15]. In this article, we report a comprehensive variable temperature and variable pressure, hyperpolarized (HP) [129]Xe NMR study in order to provide information on the correlation between chemical shift and mesopore size as well as the adsorption enthalpy of xenon on different silica and aluminium-containing silica mesoporous materials.

2. Experimental

2.1. Materials

The synthesis and characterization of MCM-41 and AlMCM-41 with 0.05 Al/(Si+Al) atomic ratio used in this work has been described elsewhere [16].

The SBA-16 sample, synthesized using Pluronic F127 ($EO_{106}PO_{70}EO_{106}$) as a surfactant, presents a distorted cubic face-centered array of cavities of 8–10 nm diameter connected through openings of ca. 2 nm [17].

Four pure silicate SBA15 (**a, b, c**, and **d**) with different pore sizes have been prepared in different experimental conditions, using Pluronic 123 triblock copolymer ($EO_{20}PO_{70}EO_{20}$) as a structure-directing agent. SBA15-a was treated in a Teflon bottle inside the oven at 100 °C for 24 h. SBA15 (**b, c** and **d**) were treated for 48 h at 60, 110 and 130 °C respectively [18]. SBA15-e and SBA15-f samples were synthesized using Brij 56 ($C_{16}EO_{10}$) as a surfactant and tetraethyl orthosilicate (TEOS) as a silica source [19]. After being stirred for 20 h, the gel solution was transferred into a Teflon bottle heated for 24 h at 60 and 100 °C, respectively.

Two Al-containing SBA15 mesoporous AlSBA-I and AlSBA-II solids with Si/Al = 10 have been prepared as described elsewhere [13,20]. The characteristics of these samples are given in Table 1.

2.2. [129]Xe NMR optical pumping set-up

[129]Xe NMR spectra were recorded on a Bruker AMX300 spectrometer operating at 83.03 MHz. The continuous flow system for production of hyperpolarized xenon was described in [9]. Variable xenon pressure spectra were taken using Xe–He mixtures containing 0.5–1000 Torr of [129]Xe polarized to ca. 1% at a total pressure of 1000 Torr. Variable temperature spectra were obtained using a 1% Xe–He mixture at a total pressure of 1000 Torr. The mixtures were delivered to the sample at a 75-cm^3 min^{-1} flow rate.

Prior to the NMR measurements samples have been compressed at 380 MPa to pellets of ca. 0.2 mm thickness and heated under vacuum at 573 K for 12 h. A number of 8–256 FIDs were accumulated with 10 µs ($\pi/2$) pulses and 1–30-s recycling delays. The [129]Xe chemical shift are referenced to the signal of xenon gas

at 10 Torr. Once the HP ^{129}Xe spectrum was recorded, the lasers were switched off and the thermally polarized (TP) xenon experiment was performed under the same conditions.

3. Results and discussion

3.1. Variable-pressure experiments

The observed ^{129}Xe chemical shift δ of xenon adsorbed on the surface can be expressed as:

$$\delta = \delta_{\mathrm{ref}} + \delta_{\mathrm{Xe}} + \delta_{\mathrm{s}} \qquad (1)$$

where δ_{ref} is the chemical shift of xenon gas at zero pressure ($\delta_{\mathrm{ref}} = 0$), δ_{Xe} is the chemical shift due to xenon–xenon collisions and δ_{s} is the contribution due to the interaction of xenon with the surface [2–4,9].

For zeolites, the chemical shift increases with the xenon pressure due to the Xe–Xe interactions inside the micropores [2]. The pressure influence on δ is however limited in mesoporous solids owing to the presence in these samples of relatively large cavities where the xenon does not spend much time at the surface and thus does not feel the wall or the other xenon atoms much. The main contribution to the chemical shift is caused by the Xe atoms adsorbed on the surface owing to their rapid exchange with free surrounding Xe atoms.

Following the analysis of Terskikh et al. [4] under fast exchange conditions and assuming that the adsorption isotherms of xenon on mesoporous materials obey Henry's law, the ^{129}Xe chemical shift of xenon adsorbed on mesoporous materials is expressed as:

$$\delta = \delta_{\mathrm{s}} / \left\{ 1 + V_m / \left(S_m\, T\, K_{\mathrm{ads}}\, R \right) \right\} \qquad (2)$$

where V_{m} is the mesoporous volume, S_{m} the mesoporous surface area, T the temperature, and K_{ads} the Henry constant.

This relationship shows the δ-independence of the equilibrium pressure. Knowing K_{ads} and δ_{s}, it is possible to obtain the volume to surface ratio, the geometry and the dimensions of the pore system [4]. Variation of δ versus xenon pressure for pure silica MCM-41 (Fig. 1) shows that the chemical shift is practically pressure-independent. Indeed, the independence of the chemical shift of xenon pressure was also observed for amorphous silica [4–5] and MCM-41 [21].

Contrary to MCM-41, a variation of the chemical shift with xenon pressure is observed for AlMCM-41, AlSBA-I, pure silica SBA15-a (**c, d** and **f** in Fig. 1). In the case of AlMCM-41, this decrease in the chemical shift can be due to the coordinatively unsaturated Al^{3+} ions, which are known to induce a strong downfield shift of adsorbed xenon [22]. The other possible explanation of the observed pressure dependence is the presence of microdefects in the walls of AlMCM-41 [16], which can also act as strong adsorption centres for xenon. So, the Equation (1) can be expressed as:

$$\delta = \delta_{\mathrm{ref}} + \delta_{\mathrm{Xe}} + \delta_{\mathrm{s}} + \delta_{\mathrm{SAS}}$$

Since the chemical composition of the surface of SBA15 samples is the same as in the case of MCM-41, the only reason for the difference in the pressure dependencies of the chemical shifts can be some factors, connected to the geometry of the adsorption sites and fast exchange of xenon between interconnected regions of different porosities. The most probable candidates for such sites are the micropores in the walls of SBA15. The presence of such microporosity in SBA15 samples under specific synthesis conditions has been well established [18]. In order to have such a behaviour of δ, the length of the micropores should be in the order of the wall thickness, which does not exceed several nanometers for SBA15, so xenon will be in fast exchange between micro- and mesopores. To explain the pressure dependence of δ for AlSBA-I and AlSBA-II, we have to take into account not only the presence of micropores [14,20], but also the influence of aluminium, as in the case of AlMCM-41.

For SBA15-b and SBA15-e, synthesized at 60 °C, the chemical shift of xenon increases with the xenon loading (Fig. 1). This suggests the presence of micropores, long enough to adsorb several xenon atoms and sufficiently large to ensure the Xe–Xe interactions. Such interactions are responsible for the positive deviation of δ. As it has been shown by Galarneau et al. [18], SBA15 samples prepared with Pluronic 123 (EO$_{20}$PO$_{70}$EO$_{20}$) as surfactant at temperatures below 80 °C present a microporosity resulting from interpenetration of the EO segments into the silica walls. This interaction decreases inversely with the synthesis temperature and leads to the disappearance of the micropores and to the formation of secondary porosity connecting adjacent pores through the walls.

^{129}Xe NMR spectrum for Xe adsorbed on SBA-16 at a pressure of 9 Torr exhibits two lines corresponding
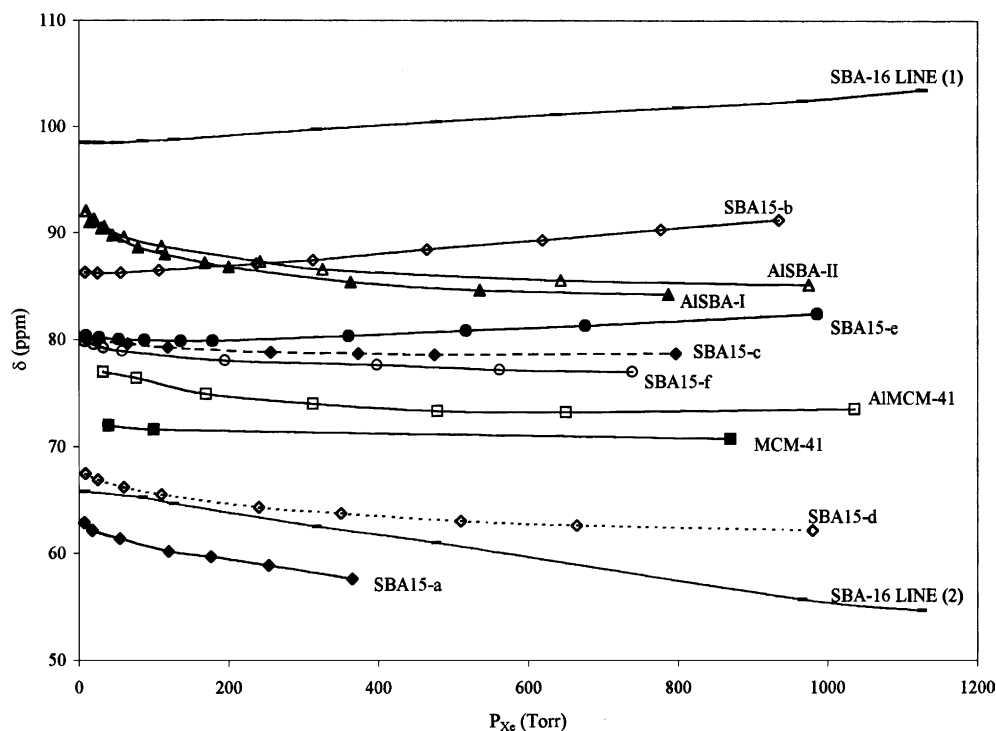
Fig. 1. Variation of [129]Xe NMR chemical shift versus xenon pressure for MCM-41, AlMCM-41, SBA-16, SBA15-a (b, c, d, e and f), AlSBA-I and AlSBA-II mesoporous solids.

to two different porosities in the sample (Fig. 2). The line (1) with $\delta = 98.5$ ppm is attributed to xenon adsorbed on the small connections. Indeed, the positive deviation of δ with xenon pressure is due to the Xe–Xe collisions inside these small pores. The line (2) with $\delta = 65.7$ ppm is attributed to the xenon adsorbed in the around 8-nm cavities. The decrease of δ with xenon
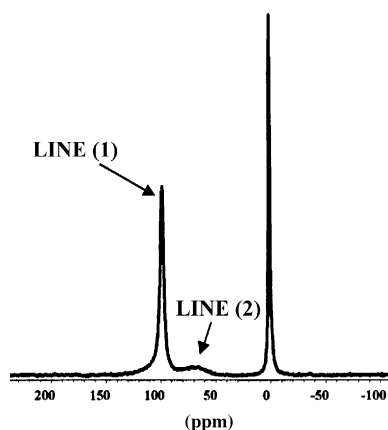
loading is due to the fast exchange between adsorbed xenon and the xenon gas in free space.

3.2. Chemical shift and pore size correlation

Empirical correlations were proposed long ago between isotropic Xe chemical shifts and the pore size (δ–D correlation) in clathrates and zeolites [3]. Attempts to extend it beyond zeolites have failed, and it has been pointed out that different correlations must exist for small pores, with a diameter less than about twice the diameter of a Xe atom, and large pores, as in the latter case one should take into account the free Xe not adsorbed on the pore walls [4,21]. Assuming that the [129]Xe NMR chemical shift of xenon adsorbed in mesoporous silica is a dynamic average between the gas and adsorbed states Equation (2) can be expressed, under fast exchange conditions, as described by Terskikh et al. [23] (Equation (3)):

Fig. 2. [129]Xe NMR spectrum of SBA-16 mesoporous solid at 9 Torr xenon pressure.

$$\delta = \delta_s / \left(1 + D/b\right) \qquad (3)$$

where the pore diameter $D = \eta\, V/S$, $b = \eta\, K\, R\, T$ and η depends on the model adopted for the pores.
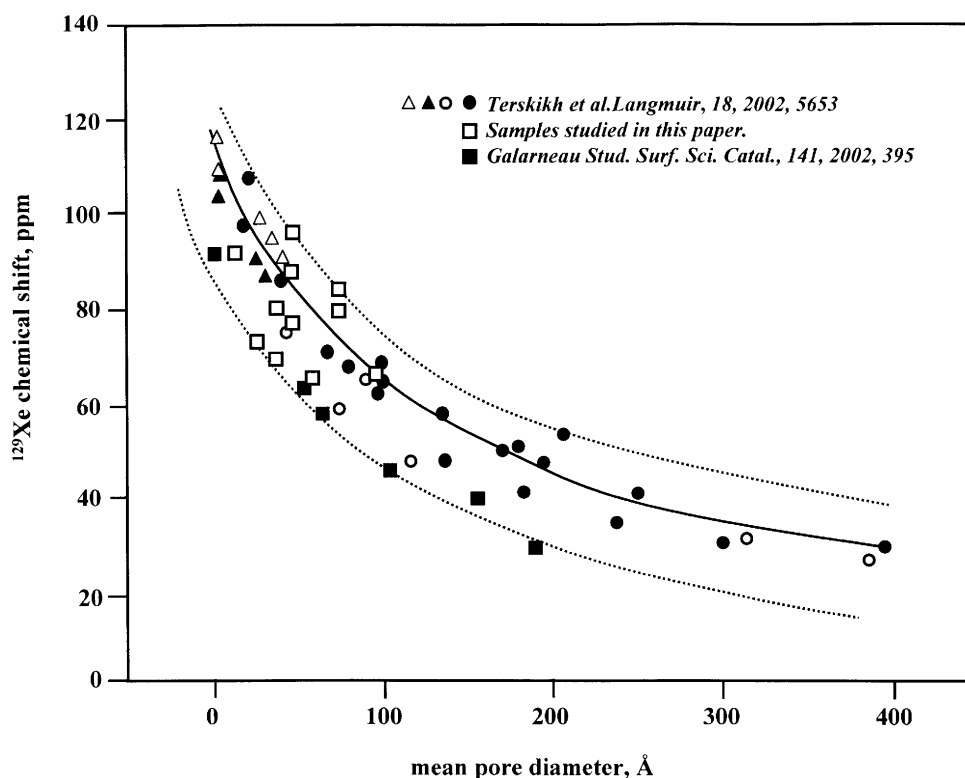
Fig. 3. Correlation between the ^{129}Xe Chemical shift and the pore size of mesoporous materials. The solid curve corresponds to the Equation (1) in [23].

^{129}Xe NMR chemical shifts versus mean pore diameters of porous silica-based materials are shown in Fig. 3, revealing an obvious relationship between δ and D. One should know that this δ–D correlation has its limitations [4,5,23]. They are mainly associated with the fact that, at ambient and higher temperatures, xenon atoms can probe a lot of distinct adsorption sites with different chemical shift values, and hence the value of the observed chemical shift cannot be directly related to a specific environment. It is also obvious that textural properties such as size and packing of the particles, as well as the chemical composition and the structure of the surface, all influence the observed chemical shift.

3.3. Variable-temperature experiments

An interesting feature of low-temperature measurements on these samples is the fact that the spectra of TP

xenon become easily detectable (within several minutes of accumulation without laser irradiation) at temperatures below 253 K, due to higher adsorption of xenon. Chemical shifts of TP xenon coincide within the experimental error with those of HP xenon, which indicates that, in our case, the spectra of HP xenon truly represent the properties of the entire sample. The integrated area of the line from adsorbed TP xenon that corresponds to the amount N_a of adsorbed xenon was corrected at different temperatures following the Curie law [9].

In the case of Henry adsorption, the amount of xenon adsorbed on the surface is [9,24] (Equation (4)):

$$N_a = K_{ads}(T)\, P\, S = \frac{k_0}{\sqrt{T}} \exp\left(-\frac{\Delta H_{ads}}{RT}\right) P\, S \qquad (4)$$

where k_0 is the pre-exponent factor and ΔH_{ads} is the adsorption enthalpy. From the temperature-

dependence of the adsorbed xenon signal intensity, it is possible to obtain the ΔH_{ads} values (Table 1) [9,24].

It is also possible to evaluate ΔH_{ads} using the observed chemical shift values in the high-temperature range. Knowing that:

$$K_{ads} = \frac{k_0}{\sqrt{T}} \exp\left(-\frac{\Delta H_{ads}}{RT}\right)$$

and in the presence of cylindrical non-intersecting pores, Equation (2) can be written in logarithmic coordinates as (Equation (5)):

$$\ln\left(\frac{1}{\delta_{obs}} - \frac{1}{\delta_S}\right) + \frac{1}{2}\ln(T) = \ln\frac{D}{4\,\delta_S\,k_0\,R} + \frac{\Delta H_{ads}}{RT} \qquad (5)$$

The value of the experimentally observed chemical shift δ depends both on δ_s and D. The independent measurements of these two parameters are needed to determine the adsorption enthalpy. The determination of ΔH_{ads} from independent measurements on TP xenon makes it possible to obtain the value of δ_s without any assumptions on the values of D. If one plots $\ln\left(\frac{1}{\delta_{obs}} - \frac{1}{\delta_s}\right) + 0.5\ \ln(T)$ versus $10^3/T$ for a material having a given δ_s value, the slope of this linear variation allows us to determine the corresponding ΔH_{ads} parameter [9,24]. Then, it is possible to plot ΔH_{ads} versus δ_s for a set of $(\Delta H_{ads}; \delta_s)$ values. Based on the value of ΔH_{ads} obtained from TP ^{129}Xe spectra, the δ_s parameter for the studied solid can be determined. The calculated values for the studied mesoporous materials are shown in Table 1. They are in a good agreement with previously published data [4,5].

4. Conclusion

The general correlation [23] between the mean pore diameter and the chemical shift of HP ^{129}Xe adsorbed on mesoporous materials is also valid for the samples studied here. The combination between HP ^{129}Xe and TP ^{129}Xe NMR data performed respectively at high and low temperatures allowed us to measure the adsorption energy and the chemical shift of xenon on the surface. The variation of ^{129}Xe chemical shift with pressure allowed us to evidence the presence of strong adsorption sites such as microporosity in the walls of several mesoporous materials.

References

[1] T. Ito, J. Fraissard, in: L.V.C. Rees (Ed.), Proc. 5th Int. Conf. on Zeolites, Naples, Italy, Heuden, London, 1980, p. 510.

[2] J.-L. Bonardet, J. Fraissard, A. Gédéon, M.-A. Springuel-Huet, Catal. Rev. Sci. Eng. 41 (2) (1999) 115.

[3] M.A. Springuel-Huet, J. Demarquay, J. Ito, J. Fraissard, Stud. Surf. Sci. Catal. 37 (1988) 183.

[4] V.V. Terskikh, I.L. Mudrakovskii, V.M. Mastikhiu, J. Chem. Soc. Faraday Trans. 89 (1993) 4239.

[5] F. Cros, J.-P. Corb, L. Malier, Langmuir 16 (2000) 10193.

[6] B.C. Grover, Phys. Rev. Lett. 40 (1978) 391.

[7] R. Seydoux, A. Pines, M. Haake, J. Reimer, J. Phys. Chem. B. 103 (1999) 4629.

[8] D. Raftery, H. Long, T. Meersmann, P.J. Cramdinetti, L. Reveu, A. Pines, Phys. Rev. Lett. 66 (1991) 584.

[9] A. Nossov, E. Haddad, F. Guenneau, A. Gédéon, Phys. Chem. Chem. Phys. 5 (2003) 4473.

[10] C.T. Kresge, M.E. Leonowicz, W.J. Roth, J.C. Vartuli, J.S. Beck, Nature 359 (1992) 710.

[11] J.S. Beck, J.C. Vartuli, W.J. Roth, M.E. Leonowicz, C.T. Kresge, K.D. Schmitt, C.R.-W. Chu, D.H. Olson, E.W. Sheppard, S.B. Mc Culler, B.J. Higgins, J.L. Shlenber, J. Am. Chem. Soc. 114 (1992) 10834.

[12] A. Corma, Chem. Rev. 97 (1997) 2373.

[13] Y. Yue, A. Gédéon, J.-L. Bonardet, N. Melosh, J.-B. D'Espinose, J. Fraissard, Chem. Commun. (1999) 1967.

[14] J.-B. D'Espinose, E. Haddad, A. Gédéon, Magnetic Resonance, Coll. & Int. Sci. NATO Series, 76, Kluwer Academic Publishers, 2002, p. 307.

[15] M. Morey, A. Davidson, G. Stucky, Microp. Mater. 6 (1996) 99.

[16] E.G. Kodenev, A.N. Shmakov, A. Yu. Derevjankin, O.B. Lapina, V.N. Romanikov, J. Mol. Catal. A 158 (2000) 349.

[17] L.A. Solovyov, O.V. Belousov, A.N. Shmakov, V.I. Zaikovskii, S.H. Joo, R. Ryoo, E. Haddad, A. Gédéon, S.D. Kirik, 3rd IMM Symposium, Jeju, Korea, 2002, p. 46.

[18] A. Galarneau, H. Cambon, F. Renzo, F. Fajula, Langmuir 17 (2001) 8328.

[19] E. Haddad, A. Lassoued, J.-L. Bonardet, J. Fraissard, A. Gédéon, Proc. 13th Int. Zeolite Conference, Montpellier, France, 2001.

[20] E. Haddad, J.-B. D'Espinose, A. Nossov, F. Guenneau, A. Gédéon, Stud. Surf. Sci. Catal. 142 (2002) 1173.

[21] M.A. Springuel-Huet, K. Sun, J. Fraissard, Microp. Mesop. Mater. 33 (1999) 89.

[22] G. Oye, M.A. Springuel-Huet, J. Fraissard, M. Stöcker, J. Sjöblom, Stud. Surf. Sci. Catal. 135 (2001) 1034.

[23] V.V. Terskikh, I.L. Moudrakovski, I.L. Breeze, R. Steven, S. Lang, C. Ratcliffe, J.A. Ripmeester, A. Sayari, Langmuir 18 (2002) 5653.

[24] A. Nossov, E. Haddad, F. Guenneau, A. Galarneau, F. Di Renzo, F. Fajula, A. Gédéon, J. Phys. Chem. B 107 (2003) 12456.